Pyroelectric infrared sensor-based thermometer for monitoring indoor objects

C. F. Tsai and M. S. Young[a)]
Department of Electrical Engineering, National Cheng-Kung University, Tainan, 701 Taiwan, Republic of China

(Received 27 March 2003; accepted 9 September 2003)

This article describes a system for measuring temperature by monitoring an object's radiation in the infrared spectrum. Using a measuring device by passing through a data acquisition interface, a long-term observation of the temperature variance of objects on a personal computer by the LabVIEW software is conducted. A special mechanism joined with a pyroelectric infrared (PIR) sensor, optical chopper, and Fresnel lens is presented in this system. This separable architecture makes the lens easily replaceable and portable. In this study, the PIR sensor into a quantitative measurement for long-term and long-distance applications with calibration equipment based on a blackbody and some electrometers was successfully applied. Experimental results show that the measuring device only has an average error rate of 1.21% in the overall range from 40 to 200 °C, and field of view is 4.58°. The results confirm that noncontacted temperature measurement using a PIR sensor is feasible. © *2003 American Institute of Physics.* [DOI: 10.1063/1.1626005]

I. INTRODUCTION

In general, fire detectors almost do not alarm unless they contact thick smoke or feel enough heat. Temperature is one of the fundamental parameters that characterize a fire accident process. To avoid the fire accident, previously knowing the information about temperature variations of some specific matter becomes a critical point.

The surface temperature of an object can be acquired directly by a contacted measurement, such as using a thermistor, thermocouple, etc. This method is more accurate than all kinds of noncontacted measuring approaches. However, it is too slow to respond to the state of emergency using contacted measurement. Besides, it is also unsuitable for a difficult-to-reach object or a dangerous place where corrosion is or electric-shock happens easily. The heat conduction is gradual, whereas the radiation propagation is very rapid. Especially when the temperature is below 400 °C then its radiation almost covers a large part of the infrared region. Hence through infrared (IR) detection, measuring the temperature of an object should be a quick and effective method.

The pyroelectric infrared (PIR) sensor has high performance for IR detection at room temperature, and it does not need to use special and expensive cooling equipment like a photon-type detector. In recent years, pyroelectric devices have been extensively used in the people's livelihood, such as intruder detecting and wisely light controlling. Several studies have touched on other applications, such as monitoring the flow in traffic, collecting people's information, etc.[1,2] Most of these usages belong to qualitative applications. However, little research has been done on quantitative measurement. Even though there are good reports on x-ray radiation measurement or tympanic thermometer,[3–5] these are only used in measuring the pulsed or the shuttled radiation power that is in a narrow range or in an enclosed environment. The main reason is that the derivative characteristic of pyroelectic devices is easily influenced by light. So, it is seldom used in the applications of remote sensing and low temperature measurement.

To solve the aforesaid problems, a chopping method was adopted in this research for two reasons: (1) the PIR sensor can be operated to get a long-term steady signal, and (2) it can also eliminate thermal drift to reduce the influence of housing temperature changes. In this study, we proposed a new mechanism where a chopper disk is put in between a lens and a sensor, and joined together with the signal conditioner. It is not only low cost and high stability, but also easy to carry. Experimental results show that this device has a good reproducibility in the measurand of noncontacted temperature.

The purpose of the proposed system is to monitor the temperature of indoor equipment, especially a power substation with embedded danger, and to aid us in recognizing the phenomenon of the temperature rise-rate or the critical temperature point. These can be taken as the important parameters to predict a possible fire accident.

II. METHOD

A. Radiation principles

Generally, as the fireproof temperature of an electric isolator is around 90 °C by the standard of IEEE, the hot spot temperature of a power transformer must be below 120 °C.[6] Besides, under the fire action, wood may start to decompose H_2O and CO_2 while the temperature is rising to between 150 and 200 °C. Wood will also start to decompose toxic gas CO when the temperature goes beyond 200 °C. In order to observe the key point of the change of temperature, the effective detection range from 40 to 200 °C was set in this study.

a)Author to whom correspondence should be addressed; electronic mail: msyoung@mail.ncku.edu.tw

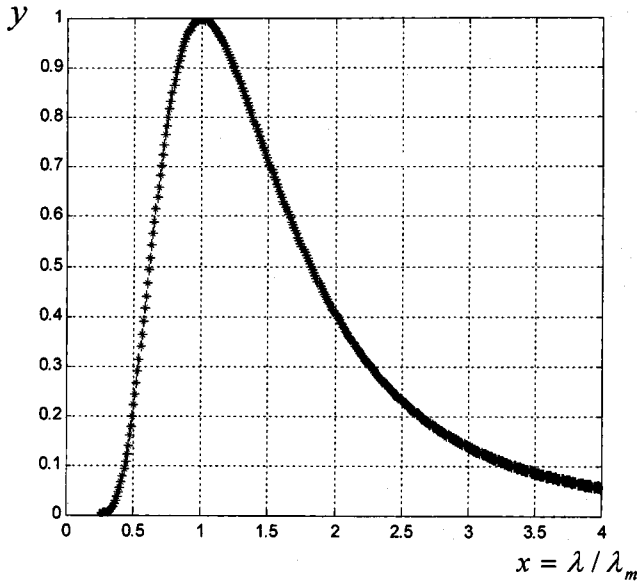

FIG. 1. A normalized Planck curve by using λ/λ_m as the variable x for finding the relative value of radiation power of any wavelength compared with that of peak wavelength.

By the Stefan–Boltzmann law, the total radiant exitance of body $M_e(T)$ is proportional to the fourth power of its surface temperature as follows:[7]

$$M_e(T)=\varepsilon\sigma T^4, \tag{1}$$

where ε denotes emissivity, σ is Stefan–Boltzmann's constant and is equal to $5.670\,32\times10^{-12}\,\mathrm{W\,cm^{-2}\,K^{-4}}$, and T is the temperature in Kelvin.

Hence we could know the surface temperature of a body by measuring its radiant power. In addition, the Wien's displacement law states that the peak wavelength of the radiation λ_m has a constant concern with the temperature T. That is,

$$\lambda_m T=2898\,\mu\mathrm{m\,K}. \tag{2}$$

In order to detect the temperature of a body's surface effectively, we use λ/λ_m as the variable x to draw the Planck curve by using the MATLAB software as shown in Fig. 1. The value y can be derived as follows:

$$\begin{aligned} y&=\frac{M_{e,\lambda}(\lambda,T)}{M_{e,\lambda}(\lambda_m,T)}\\ &=\frac{2\pi hc^2\lambda^{-5}}{\exp(hc/\lambda kT)-1}\Big/\frac{2\pi hc^2\lambda_m^{-5}}{\exp(hc/\lambda_m kT)-1}\\ &\approx 142.3\frac{x^{-5}}{\exp(4.965/x)-1}, \end{aligned} \tag{3}$$

where $M_{e,\lambda}(\lambda,T)$ is the spectral radiant exitance, and $M_{e,\lambda}(\lambda_m,T)$ is the peak radiant exitance.

By Eq. (3) and the Plank curve shown in Fig. 1, it is found that the half power point falls around 0.614 and 1.81. Furthermore, by Eq. (2), the evaluated peak wavelength covers the range of 6.1–9.2 μm, that is part of the IR region. So we chose the PIR sensor IRA-E410S1 made by Murata Co.,

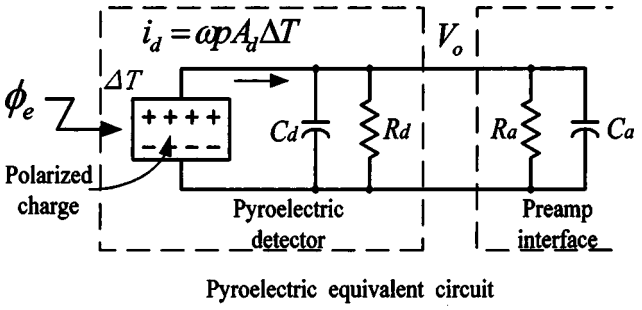

FIG. 2. The equivalent circuit of the pyroelectric device.

which has a uniform response at 1–20 μm, to cover the larger part of irradiance power, and has a better signal-to-noise ratio.

B. The characteristics of the PIR device

For IR detection, there are two types of methods based on photon effect and thermal effect, respectively. Although the former has a higher sensitivity and a fast response time of less than 1 μs,[8] they have an even more restricted spectral response and need very expensive cooling equipment. However, thermal-type devices, including thermopile, bolometer, and PIR sensor, are able to work at room temperature. The PIR sensor is the cheapest one among all IR products, whether photon type or thermal type, and only costs less than one-tenth of a thermopile.

The PIR sensor consists of pyroelectric material, such as TGS, $BaTiO_3$, etc., which possesses a spontaneous polarization depending on the change of temperature. It acts like an electric capacitance and is a derivative detector. The equivalent circuit of the PIR sensor is shown in Fig. 2, and R_d, C_d stands for the equivalent resistance and capacitance of sensor, respectively. The polarization charge produced by a temperature change is related to the irradiation power ϕ_e received by the detector. It causes a current i_d that is $\omega pA_d(\Delta T)$. The output voltage V_o, equaling the current i_d multiplied by the impedance, can be derived as follows:

$$V_o=\frac{i_d R_d}{\sqrt{1+\omega^2R_d^2C_d^2}}=\frac{\omega pA_dR_d(\Delta T)}{\sqrt{1+\omega^2R_d^2C_d^2}}, \tag{4}$$

where p is the pyroelectric coefficient, ω is the radian frequency, and ΔT is the difference of detector temperature T_d and ambient temperature T_a. By the heat-balance equation given as follows:

$$\phi(t)=C_T\frac{d(\Delta T)}{dt}+\frac{\Delta T}{R_T}+A_d\sigma(T_d^4-T_a^4), \tag{5}$$

ΔT can be found as

$$\Delta T=\frac{R_T\phi_e}{\sqrt{(1+\omega^2\tau_T^2)}}. \tag{6}$$

Substituting ΔT into Eq. (4), we can find that it is a bandpass form as shown in Eq. (7),

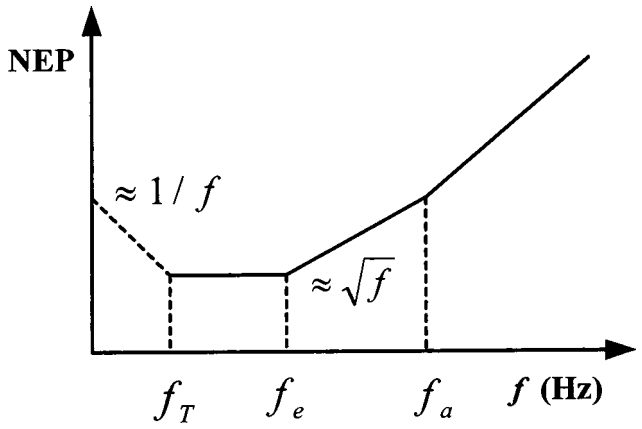

FIG. 3. Variation of noise equivalent power of the adopted pyroelectric device versus frequency.

$$V_o = \frac{\omega p A_d R_d}{\sqrt{1+\omega^2 \tau_E^2}} \times \frac{\varepsilon \phi_e R_T}{\sqrt{1+\omega^2 \tau_T^2}}, \tag{7}$$

where τ_E is the electrical time constant $(R_d C_d)$, τ_T is the thermal time constant $(R_T C_T)$, and ϕ_e is the incident radiant power.

The PIR sensor is suitable for working at the frequency from 0.1 to 100 Hz.[7] Usually the response of the device almost has a slope of -20 dB/decade for frequencies higher than 1 Hz. Because the PIR sensor responds to the rate of change of temperature dT/dt, it is suitable to measure pulse-type radiation power.

There are three main noise sources associated with the PIR sensor. They are thermal noise, Johnson noise, and preamplifier noise. Figure 3 shows the plot of the noise equivalent power (NEP) versus frequency. In general, the flat response is from 10 to 40 Hz for the lowest NEP value. It has an obvious influence by $1/f$ noise below 10 Hz, and a noise value of about 20 nV/$\sqrt{\text{Hz}}$ that is proportional to $\sqrt{f}$ above 40 Hz, but dropping to 2 nV/$\sqrt{\text{Hz}}$ above 1 kHz.[9,10] Here we adopted the chopped-radiation method that combines a chopper with a high Q bandpass filter (BPF) to obtain a better signal-to-noise ratio.

C. Experimental structure

The simplified experimental process is illustrated in Fig. 4. It includes a blackbody (BB), a PID (proportional, integral and derivative) controller, a blacked IR radiator, and a measuring unit (MU). The BB (ISOTECH, Model-976), with the diameter of the bore being 60 mm ϕ and a controllable temperature range of 35–550 °C, is used to calibrate the temperature scale of the MU. The IR radiator, with an emissivity of about 0.93, is controlled by a PID controller (Gi-da Co., MC2838) and used as a measured target. Its radiant area is 125 mm ϕ in diameter; and it works at a 300 W (220 V) power.

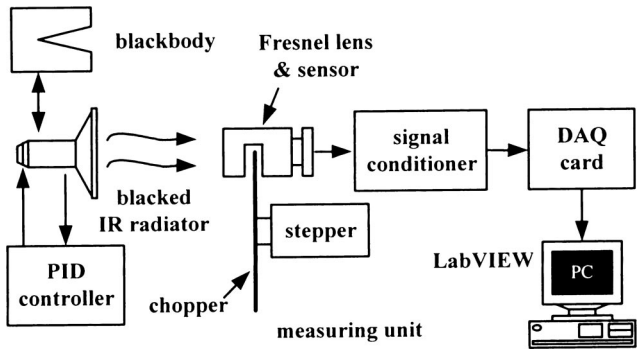

FIG. 4. Block diagram of the overall experimental system.

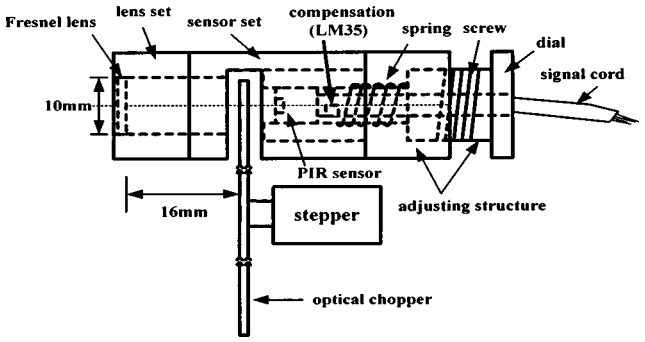

FIG. 5. Diagram of the optical structure including lens set, PIR sensor, and chopper.

In order to measure efficiently, we chose a suitable distance between the source and the detector within the field of view (FOV), that is, the BB and the PIR radiator are 30 and 50 cm away from the MU, respectively. The collected IR signal, coming from the Fresnel lens and detecting from the PIR sensor, passes through the signal conditioner shown in Fig. 9. Finally, the LabVIEW(Laboratory Virtual Instrument Engineering Workbench) software on a PC through a DAQ card was used to view results. The DAQ card, made by National Instrument Corporation, is a multifunctional input-output device with a sampling rate up to 100 kSa/s and 12-bit performance on analog inputs. So the resolution of the implemented system is within 0.05 °C in this study.

D. Optical systems

The optical structure of the MU is shown in Fig. 5, which consists of a lens set, a PIR sensor, and an adjustable mechanism made of copper as shown in Fig. 6. The separable lens set can be conveniently replaced by the other set with a different focal length when it is used for the other purpose. The chopper is placed in front of the target to get a higher accuracy. But, this structure is only suitable for short-distance application, such as the characteristic test of an IR element. Furthermore, the chopper disk should be put in between the lens and the sensor, then joined together. The Fresnel lens set, with a diameter D_{lens} of 10 mm and a focal length f of 20 mm, is made up of the polyethylene material and its characteristic is shown in Fig. 7. The polyethylene has about 70% transmittance from 1 to 30 μm except for a minority of spectrum band.[7]

Because the PIR sensor IRA-E410S1 has a detected area A_d of 1.6 mm φ, and is placed closely to the focal of the lens, the FOV is about 4.58° approximated by the following formula:[11]

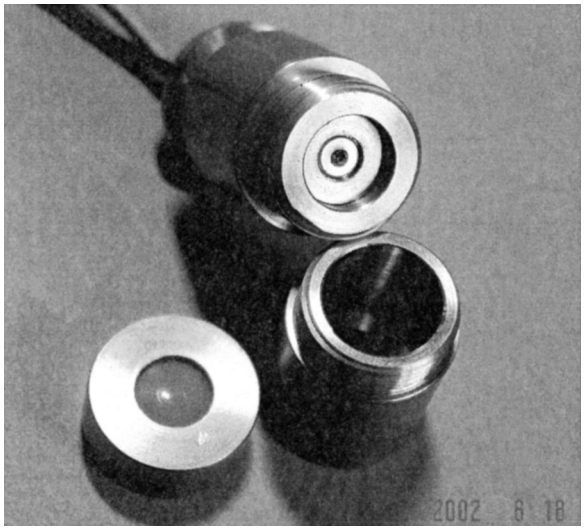

FIG. 6. A photograph of the optical structure made of copper that includes a lens and a PIR sensor set.

$$\mathrm{FOV}_{\text{half-angle}} \approx \left| \tan^{-1}\left(\frac{d_s/2}{f}\right) \right| = 2.29°, \tag{8}$$

where d_s is the detected diameter of the sensor. By Eq. (8), we can find the optical resolution, i.e., the (distance to spot) D:S (spot diameter) ratio of 12.5:1.

The chopper disk is put behind the lens to avoid the influence caused by thermal drift. Furthermore, the chopping method can be used to produce a stable and pulse-like signal continuously. The chopper, with a diameter D_c of 80 mm, is a disk partitioned into four parts and driven by a stepper as shown in Figs. 8(a) and 8(b). It works at a frequency of 8 Hz and is placed near the PIR sensor 16 mm behind the lens. It chops the incoming light about 4 mm in diameter, which is much smaller than the tooth-width (TW, about 27.5 mm) of the chopper. Therefore the modulation factor (MF)[12] can be found by using Eq. (9) as follows:

$$\mathrm{MF} = \frac{\sqrt{2}}{\pi} \times F\left[\frac{-N}{2}, \frac{N}{2}, 2, \left(\frac{d}{D}\right)^2\right] \approx 0.447, \tag{9}$$

where $F[\cdot]$ is the hypergeometric function, N is the number of tooth-slot pairs (4), D is the diameter of the chopper (in 70 mm), and d is the aperture diameter (in 4 mm). The value of MF is close to 0.45, which is the value of an ideal square wave.

Besides, the sensor is located closely to the focus, and the incoming light is focused by a movable mechanism, which can provide continuously sharp imagery. By Eq. (4), if the sensor works under a steady frequency condition, then its output V_o will be proportional to the change in temperature of sensor (ΔT). By Eqs. (5)–(7), the temperature change depends on the incident radiant power received by detector. The detecting power ϕ is described by the following equations:[8]

$$\phi \approx \frac{L'(T_s) A_d A_l}{f^2} = \frac{L'(T_s) A_d \pi}{4(f/D_{\text{lens}})^2}, \tag{10}$$

where $L'(T_s)$ is the Lambert of target at temperature T_s, A_l is the cross area of the lens, A_d is the cross area of the detector, and D_{lens} is the diameter of the lens. By Eq. (10), the smaller the f-number is, the better sensitivity can be obtained. However, long focal length gives a narrower FOV and a better resolution.

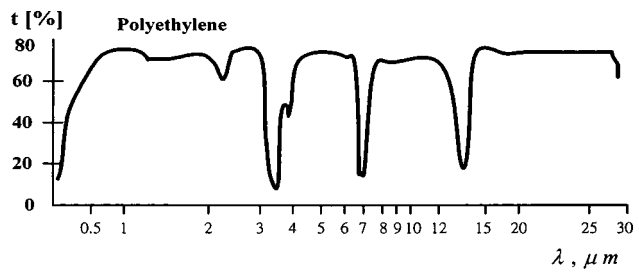

FIG. 7. The transmittance of polyethylene in the infrared region.

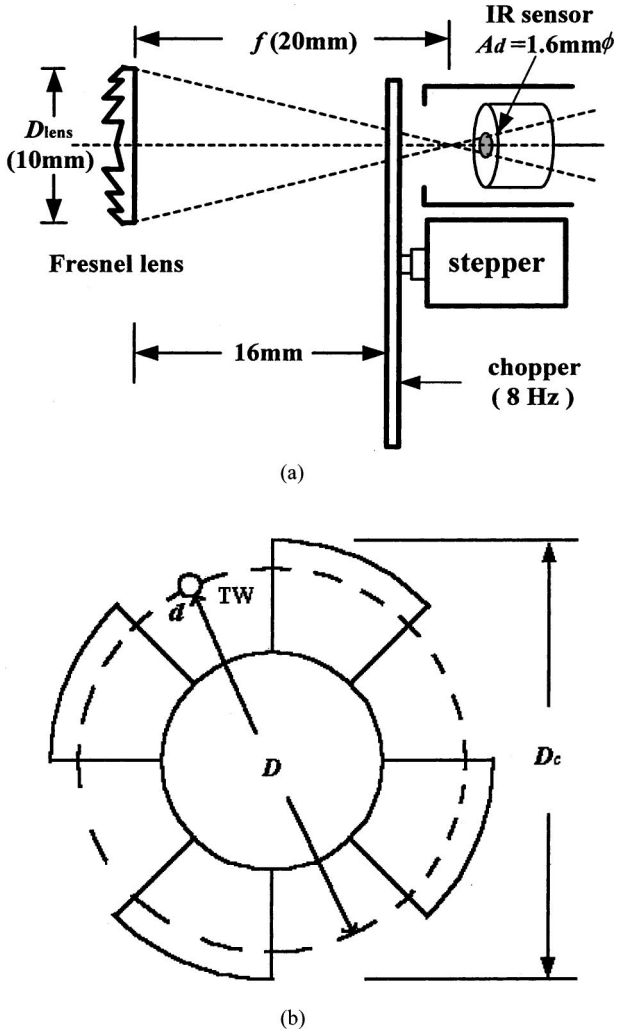

FIG. 8. (a) Diagram of lens and chopper setup. (b) Configuration of the chopper disk.

E. Circuit system

In this study, the simplified block diagram of the MU is shown in Fig. 9. The main function of the MU is to transfer the temperature change from 40 to 200 °C into dc output

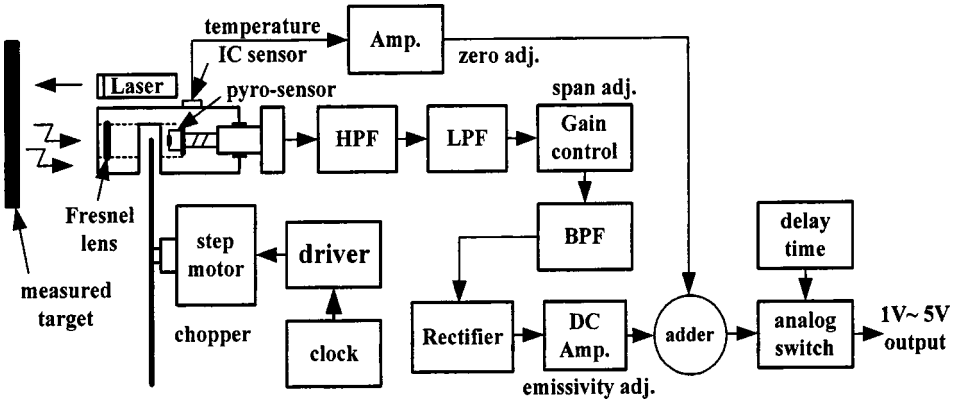

FIG. 9. Block diagrams of the measurement unit that includs lens set, chopper, and condition circuits.

from 1 to 5 V. By considering the practical condition, we modify Eq. (10) for the signal picked up by the sensor as follows:

$$V_s(T_s)=\Re_v\times \mathrm{MF}\times\tau\times\varepsilon\int_1^{20}L'(\lambda,T_s)d\lambda\,\frac{A_dA_l}{f^2}, \qquad (11)$$

where $\Re_v$ is the responsivity of sensor, and τ is transmittance of the incident light.

By the data sheet, the sensor's sensitivity with an output V_s (500 K, 1 Hz, 1 Hz) of 3.0 mV_{pp} almost decays linearly with frequency. Assume that the chopping frequency is 8 Hz, the sensor's output can be estimated as follows:

$$V_s(T_s,\,8\ \mathrm{Hz})\approx V_s(T_t,\,1\ \mathrm{Hz})\times\frac{\Re_v(T_t,\,8\ \mathrm{Hz})}{\Re_v(T_t,\,1\ \mathrm{Hz})}\times\frac{L'(T_s)}{L'(T_t)}$$
$$\times\frac{\mathrm{MF}_s}{\mathrm{MF}_t}\times\frac{A_l}{A_w}\times\tau\times\varepsilon, \qquad (12)$$

where subscripts *s*, *t*, *l*, and *w* stand for the measured source, sensor under tested condition, lens, and sensor's window, respectively.

Considering the absorbance of the atmosphere and the decay of passing through a lens, we estimate that the transmittance τ of the incident power is about 0.6. The emissivity of the BB is 0.995. By Eq. (12), if the measured temperature T_s is 200 °C, the maximum output of the sensor will be about 2.89 mV_{pp} in a 25 °C environment. Thus if the eimissivity is adjustable in the range of 0.1 to 1.0, we set the total gain between 3 020 and 5 370 to obtain the output of dc 5 V.

A Lock-in amplifier is usually used to extract periodic signals from noise in the chopping method. However, the chopper must provide a clean synchronous reference signal using a photo-interrupter. This will increase the complexity of the set up work. Hence after the signal is flatly amplified over frequencies of 3–15 Hz, a second order BPF was adopted to substitute the lock-in amplifier. The BPF is a multiple-feedback filter, called the Delyiannis–Friend filter, as shown in Fig. 10. The transfer function of this filter is given as follows:

$$\frac{V_o}{V_i}=T(s)=-\frac{s\dfrac{1}{C_2R_1}}{s^2+s\left(\dfrac{1}{C_2R_3}+\dfrac{1}{C_1R_3}\right)+\dfrac{(R_1+R_2)}{C_1C_2R_1R_2R_3}}. \qquad (13)$$

In Fig. 10, if C_1 equals C_2, the values of R_1, R_2, and R_3 can be calculated by the following equations:

$$Q=\frac{1}{2}\sqrt{\frac{R_3}{R_p}},\quad G_o=-\frac{R_3}{2R_1},\quad f_o=\frac{1}{2\pi\sqrt{C_1C_2R_pR_3}},$$

where $R_p=R_1//R_2$. Here a Bi-FET operational amplifier was adopted to implement the BPF with its center frequency being 8 Hz, $Q=6.0$ and $G_o=3.0$. It can eliminate the high-order harmonics caused from the chopper modulation.

The chopping frequency is produced from the stepper, which has a 1.8° step angle. Because the stability of the chopping frequency will influence the accuracy of the measured results, it is important that the clock frequency of the stepper be kept in a fairly stable condition. To reduce the sensitivity coming from the oscillator drift, the clock frequency is divided by a decade counter and then sent into the motor driver.

A temperature sensor, which is put inside the measuring mechanism to measure the housing temperature of the PIR device, is used for compensating the PIR output values to obtain the absolute temperature of objects. Since the signal

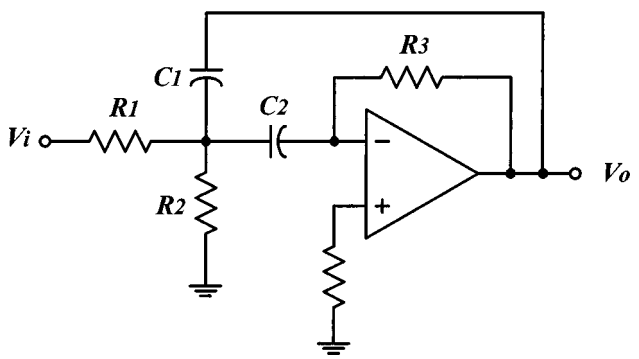

FIG. 10. A bandpass filter using a multiple-feedback structure.

TABLE I. A list of the measured results and errors vs the measured BB's temperature.

Set temp. (°C)	Measured results (°C)			Measurement errors (%)	
	average temperature	maximum temperature	minimum temperature	average	maximum
40	40.02	41.264	39.153	0.05	3.16
50	49.67	50.363	49.02	−0.66	0.73
60	60.143	62.207	57.603	0.24	−4.00
70	70.746	72.496	68.467	1.07	3.57
80	80.972	83.078	79.172	1.21	3.85
90	89.134	91.239	86.341	−0.96	−4.07
100	100.651	102.684	98.312	0.65	2.68
110	108.672	112.429	106.412	−1.21	2.21
120	119.637	123.304	118.012	−0.30	2.75
130	129.218	133.576	127.164	−0.60	2.75
140	139.726	143.208	137.902	−0.20	2.29
150	151.144	154.232	146.652	0.76	2.82
160	161.734	164.106	158.393	1.08	2.57
170	168.251	173.816	166.549	−1.03	2.24
180	179.562	182.295	176.592	−0.24	−1.89
190	192.017	194.356	186.729	1.06	2.29
200	200.182	202.49	198.274	0.09	1.25

picked up from the PIR sensor is unstable transiently when power is just turning on, it must be delayed about 30 s before it is sent out.

III. SYSTEM TESTING AND THE RESULTS

A. Calibration and measurement

The calibration procedure is divided into four steps. First, offset adjustment has to be done for each operational amplifier, especially in the last two stages after BPF, and let its output be zero when no input appears. Second, using a contacted-type thermometer (Yokogawa, TM20) to measure the sensor housing temperature with a *K*-type thermocouple and to calibrate the gain of the compensation circuit, we let it get a sensitivity of 25 mV/°C. Third, by fine-tuning the dial of the adjustable structure shown in Fig. 5, it can be expected to obtain a maximum sensitivity. Finally, the zero and span calibration was done within the measuring range.

The MU was calibrated by means of the BB with constant temperature, electrometers such as a 5 1/2 digital multimeter (Advantest R6450), and a digital oscilloscope (Agilent 54621A). We set the lens of the MU shown in Fig. 9 to face the BB's bore keeping 30 cm between them, and furthermore use a laser to point at it to confirm the target. After taking a thorough calibration between zero and span repetitiously, we adjust the dc output of the MU to be 1 and 5 V, respectively, for the BB's temperatures of 40 and 200 °C. The temperature compensated circuit is adopted to accomplish the adjustment of zero. The gain controller is used to set the total gain for the span of the measuring range. Here the sensitivity is 25 mV/°C.

A preliminary measurement is conducted by using the blacked IR radiator as a target with a distance of 50 cm away from the lens and adopting the PID controller to control the radiated power. The measurement results are taken in 1 s intervals and sent into the computer through a DAQ-1200 card under control of the LabVIEW software.

B. The measured results

In order to test the performance of the MU, we used the MU to measure the BB's temperature at an interval of 10 °C within the measuring range, and recorded it continuously by the LabVIEW software. Table I shows a list of the measured results that include maximum, minimum, average value, and errors. Figure 11 shows the plot of the measured results versus the set temperature. The data of each point on the curve

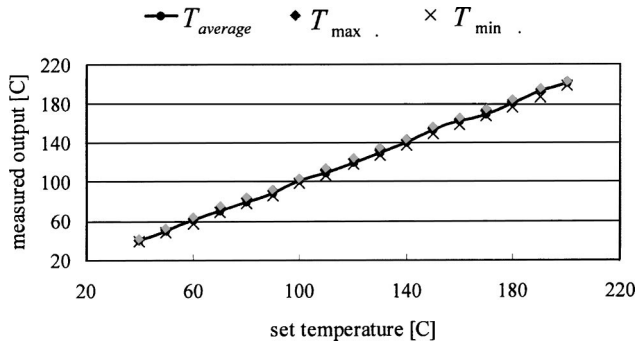

FIG. 11. Plots of the measured results from Table I. Symbols ◇ and × represent the maximum and minimum values of the measured temperature, respectively.

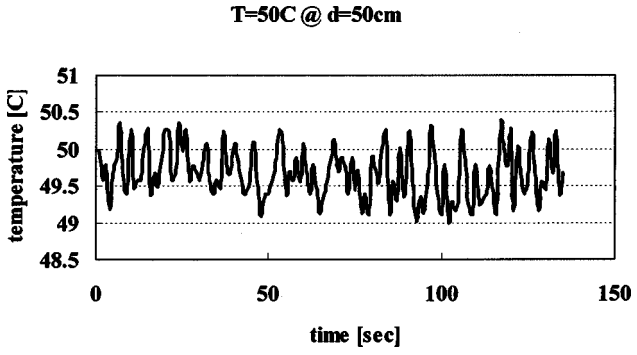

FIG. 12. A measuring history recorded by using LabVIEW software when BB was set at 50 °C.

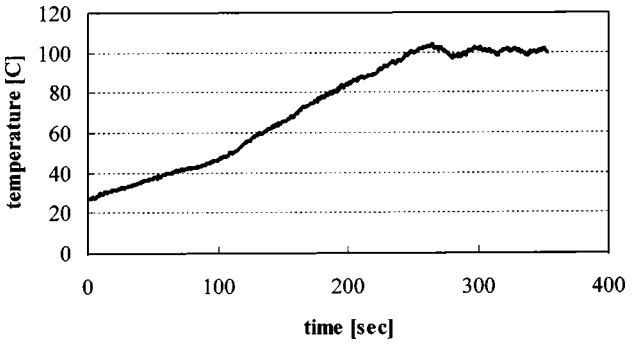

FIG. 13. A measuring history of the PID-controlled radiator heated from room temperature.

shown in Fig. 11 is an average value calculated from a number of results measured continuously during 2 min, similar to the example of measuring $T=50\,^{\circ}\mathrm{C}$ as shown in Fig. 12.

In Table I and Fig. 11, the results show that the MU has an average relative-error within 1.21% for covering the measurement range. The maximum error is about 4.0% (deviation of 2.65 °C) appearing on which temperature is set at 90 °C.

Figure 13 shows a measuring history that the blacked IR radiator was being heated from room temperature (about 27.3 °C) and was controlled at 100 °C by the PID controller. The curve shows that the temperature of the blacked IR radiator gradually settled after it had been heated for 5 min. This experimental example illustrates that the MU is effective in a practical measuring job.

IV. DISCUSSION

A novel thermometer based on a PIR sensor and related infrared techniques has been successfully employed to measure the temperature of specific matter. The experimental results show that the PIR sensor can be used for quantitative analysis with high performance. This design is complicated to harmonize with an optical chopper, but the structure may be minimized by a micromachined technique.[13] Besides, it is low cost, so this technique is worthy to develop. Some attention should be paid to discuss the following: (1) This device is effective for a slow and gradually rising temperature, but it is only suitable for indoor operation. (2) It will result in an error signal when a sudden light (for example, turning on or turning off the light, or the change of sunlight) or a sudden heat source (such as people invading) appears during the measuring process. However, using a differential detecting method with a structure-modified lens may reduce the error signal. On the other hand, this function may also be offered to detect a spark. (3) As optical chopping is the important factor of accurate detection, the steadiness of the chopping frequency has to be kept. (4) The structure of the lens must include an effective antidazzling screen and a fine adjustable focus. (5) High temperature detection is easier than low temperature detection. The reason is that the measurement may be easily influenced by ambient temperature, especially the heat convection caused from the stepper without appropriate isolation. Therefore the technique of temperature compensation is very important.

To standardize the device as a measuring unit, we may also use a voltage-to-current converter, such as XTR110, to convert the output of the MU into the current output of 4 to 20 mA, which is an industrial standard. Thus the MU can be portable and easily combined with the other system.

[1] T. M. Hussain, A. M. Baig, T. N. Saadawi, and S. A. Ahmed, IEEE Trans. Veh. Technol. **44**, 683 (1995).
[2] N. Yoshiike, K. Morinaka, K. Hashimoto, and M. Kawaguri, Sens. Actuators A **77**, 199 (1999).
[3] A. A. de Carvalho and S. Mascarenhas, IEEE Trans. Electr. Insul. **27**, 835 (1992).
[4] C. Furio, J. Int. Measurement Confederation **16**, 239 (1995).
[5] M. Ou-Yang and J. S. Shie, Appl. Opt. **37**, 2708 (1998).
[6] "Guide for loading mineral-oil-immersed transformers," IEEE Std. C51.91-1995.
[7] G. Gaussorgues and S. Chomet, *Infrared Thermography* (Chapman and Hall, London, 1994), pp. 12, 117.
[8] E. H. Putley, Phys. Technol. **4**, 202 (1973).
[9] E. L. Dereniak and D. G. Crowe, *Optical Radiation Detectors* (Wiley, New York, 1984), pp. 9, 174.
[10] G. Baker, D. E. Charlton, and P. J. Lock, Radio Electron. Eng. **42**, 260 (1972).
[11] E. L. Dereniak and G. D. Boreman, *Infrared Detectors and Systems* (Wiley, New York, 1996), p. 13.
[12] J. David Vincent, *Fundamentals of Infrared Detector* (Wiley, New York, 1990), p. 138.
[13] Th. Kraus, M. Baltzer, and E. Obermeier, Conference on solid-state sensor and actuators, 1997 (unpublished), p. 67.